

# Simulation of the impact of humidity on the species generated by a one-dimensional discharge of helium gas

Zahra Soltani<sup>1</sup> , Ramin Mehrabifard<sup>2</sup> , Fatemeh Rezaei<sup>1,\*</sup> ,  
Mohammad Mohsen Hatami<sup>1,\*</sup> , Hamed Soltani<sup>3</sup>

<sup>1</sup>Department of Physics, K. N. Toosi University of Technology, Tehran, Iran.

<sup>2</sup>Division of Environmental Physics, Faculty of Mathematics, Physics and Informatics, Comenius University, Mlynská dolina, Bratislava, Slovakia.

<sup>3</sup>Department of Atomic and Molecular Physics, Faculty of Basic Sciences, University of Mazandaran, Babolsar, Iran.

\*Corresponding author: [m\\_hatami@kntu.ac.ir](mailto:m_hatami@kntu.ac.ir), [fatemehrezaei@kntu.ac.ir](mailto:fatemehrezaei@kntu.ac.ir)

## Original Research

## Abstract:

Received:  
27 January 2024  
Revised:  
5 April 2024  
Accepted:  
16 May 2024  
Published online:  
25 May 2024

© The Author(s) 2024

Dielectric barrier discharge (DBD) plasma has several applications in different fields. One of these fundamental applications is medical usages, where various methods are employed to improve the plasma treatment process. The combination of different gases is one of the important strategies to improve the performance of plasma in treatment. In this paper, the optimized plasma parameters for one-dimensional radiofrequency discharge produced at low pressures in a helium gas combination is studied. In this research, the optimal combination of H<sub>2</sub>O and He is identified to attain the highest amount of reactive oxygen species (ROS). Considered mixture are 5, 10, 15 and 20 percent of H<sub>2</sub>O for one dimensional helium gas discharge. The results show that the parameters of the output plasma are highly dependent on the composition of the input gases. It is found that the greatest concentrations of H<sup>+</sup>, He<sup>+</sup>, Hes (excited helium), and OH densities are observed when the H<sub>2</sub>O percentage was at 10%. Moreover, the density distributions of various species and the temperatures of electrons are numerically calculated during the electrical discharge process. These findings provide useful knowledge on how to optimize plasma parameters for biomedical applications, which may lead to improved treatment results in several therapeutic areas.

**Keywords:** Cold plasma; DBD; Gas mixture; Plasma simulation; Plasma medicine

## 1. Introduction

The plasma medicine is a relatively recent issue which offers novel approaches to treat a wide range of illnesses. Due to the unusual quality and extended range of medical applications, including bio-sterilization [1], skin regeneration [2], wound healing [3], teeth whitening [4], blood coagulation, cancer cells treatment [5–7], and engineering of biomaterials and tissues [8], cold plasma discharge produced at atmospheric pressure has paid more attention in recent years. Generally, cells, tissues, and organs can all be treated employing the so-called cold atmospheric plasmas. The term “cold” describes a crucial characteristic of particular types of plasma, such as the fact that the temperature of the ions and other heavy species present in the plasma is much lower than that of the plasma’s electrons [9, 10].

Dielectric barrier discharge (DBD) offers a higher intensity, more flexible, and regulated discharge in comparison to other plasma sources which is used by the majority of biomedical devices utilizing in the cold plasma discharge [11]. A lot of literatures has been focused on identifying and analyzing the plasma properties and active species during performing successful experimental research on atmospheric pressure plasma applications in surface treatment, engineering [12, 13], processing technology, and sterilizing [14, 15]. Additionally, different research groups have studied on simulating DBD plasmas at atmospheric pressure. For instance, Gadkari et al. [16] used a 2-D fluid model in COMSOL Multiphysics to simulate a co-axial DBD plasma reactor in pure helium. They examined how partial packing affected the helium dielectric barrier discharge’s properties.

In addition, Pan et al. [17] numerically studied on different features of the atmospheric-pressure  $\text{CF}_4$  plasma in a dielectric barrier discharge using the fluid model. They obtained the plasma parameters in steady state. Furthermore, Abidat et al. [18] investigated a one-dimensional model of atmospheric pressure helium gas dielectric barrier discharge with COMSOL Multiphysics simulation. They reported the effect of dielectric coefficient and distance between electrodes on Lissajour image. Golubovskii et al. [19] used the numerical methods to study the spatiotemporal properties of the homogeneous barrier discharge in helium. They utilized a one-dimensional fluid model to investigate how the main processes affect the discharge via rate constants. Moreover, they extracted the plasma parameters in steady state.

Entertally, combining gases is one of the key methods to enhance the plasma performance in medical applications [20–22]. This is because using different gas combinations can produce other active species that are beneficial for medical applications. Employing various types of gases with different compositions is one of the ever-toughest techniques in plasma modeling. Therefore, in this study, a simulation is performed for exploring of inlet gas combination portion in cold plasma. Different portions of  $\text{H}_2\text{O}$  are mixed with helium gas and plasma characteristics had been investigated. As a result, the best and effective combination of these two gases was determined for medical applications.

## 2. Theoretical equations

### 2.1 DBD simulations in sterilization process

In this section, the governing fluid dynamic equations in the DBD simulation for sterilization purpose are described. In order to account for the reactions of various species, and as well as the rate of production and losses at the electrode surfaces, surface chemistry was applied [23]. The pair of propulsion and propagation equations were solved to compute the electron density and electron mean energy. The electron continuity equation and the flow equation can be explained by Equations (1) and (2), respectively as below:

$$\frac{\partial n_e}{\partial t} + \nabla \cdot \Gamma_e = R_e - (\mathbf{u} \cdot \nabla) n_e \quad (1)$$

$$\Gamma_e = -(\mu_e \cdot \mathbf{E}) n_e - \mathbf{D}_e \cdot \nabla n_e \quad (2)$$

where,  $n_e$  represents the electron density,  $E$  is electric field,  $D_e$  indicates the electron diffusion coefficient,  $\Gamma_e$  is electron flux,  $u$  is average species fluid velocity, and  $R_e$  represent the rate of electron creation.

It should be mentioned that two terms construct the electron flux: i) one term is originated from the electric field, and ii) the other is created from the density gradient. Equation governing on the electron energy density can be calculated by:

$$\frac{\partial n_\epsilon}{\partial t} + \nabla \cdot \Gamma_\epsilon + \mathbf{E} \cdot \Gamma_\epsilon = R_\epsilon - (\mathbf{u} \cdot \nabla) n_\epsilon \quad (3)$$

$$\Gamma_\epsilon = -(\mu_\epsilon \cdot \mathbf{E}) n_\epsilon - \mathbf{D}_\epsilon \cdot \nabla n_\epsilon \quad (4)$$

where the energy received by the electron from the electric field is denoted by the  $\mathbf{E} \cdot \Gamma_\epsilon$ . In addition, the energy rate

resulting from inelastic collisions can be expressed by the following equations:

$$R_e = S_{en} + \frac{Q + Q_{gen}}{q} \quad (5)$$

$$D_e = \mu_e T D_e = \mu_e T_e \mu_\epsilon = \frac{5}{3} \mu_e \quad (6)$$

In above equation,  $u_e$  is the energy mobility, and  $Q_{gen}$  is the thermal source,  $S_e$  is the power dissipation,  $Q$  is the primary source of heat, and  $q$  is the electron charge. It should be mentioned that due to knowing that the electron source could be determined from the Townsend coefficients must be used as:

$$R_e = \sum_{j=1}^M x_j a_j N_n |\Gamma_e| \quad (7)$$

where,  $M$  is the number of reactions,  $x_j$  is the molar percentage of the target species for the reaction  $j$ ,  $a_j$  is the Townsend coefficient for the  $j$  process, and  $N_n$  is the total number of the neutral species considering that  $p$  is the number of non-elastic collisions of an electron.

$$R_e = \sum_{j=1}^p x_j a_j N_n |\Gamma_e| \Delta \epsilon_j \quad (8)$$

here,  $\Delta \epsilon_j$  represents the energy released through the  $j$  reaction. Generally, for each mass fraction in non-electron species, the following equations must be solved:

$$\rho \frac{\partial w_k}{\partial t} + \rho (\mathbf{u} \cdot \nabla) w_k = \nabla \cdot \mathbf{J}_k + R_k \quad (9)$$

where,  $w_k$  is the ion density and  $J_k$  is the ion energy flow. The Equation (10) can be utilized for determining the electrostatic field as follows:

$$\nabla \cdot (\epsilon_0 \epsilon_r \mathbf{E}) = \rho \quad (10)$$

where,  $\epsilon_r$  is the relative dielectric constant and  $\epsilon_0$  is the permittivity of the vacuum. The following equations explains the boundary conditions for electron flux and energy flux as bellows:

$$-\hat{n} \cdot \Gamma_e = \left( \frac{1}{2} v_{eth} n_e \right) - \sum_p \gamma_p (\Gamma_p \cdot \hat{n}) \quad (11)$$

$$-\hat{n} \cdot \Gamma_\epsilon = \left( \frac{5}{6} v_{eth} n_e \right) - \sum_p \epsilon_p \gamma_p (\Gamma_p \cdot \hat{n}) \quad (12)$$

The electron is produced according to secondary emission, as shown by the second term on the right side of Eq. (11). Here,  $\Gamma_p$  is the secondary emission coefficient. It should be noted that the second term in Equation (12) is the secondary emission energy flux, where  $\epsilon_p$  is the mean energy of the secondary electrons.

Ions and excited species are neutralized particles on the electrode surface through the surface reactions. The coefficient  $\beta_j$  which determines the probability of  $j$  species functioning is used to imitate the surface interactions on the electrodes. The conjugation equation for the discharge's ion species is expressed as follows:

$$\frac{\partial n_i}{\partial t} + \nabla \cdot (n_i \mathbf{u}) = -\nabla \cdot (\mu_i n_i q_i \nabla \phi - D_i \nabla n_i) + S_i \quad (13)$$

where,  $\phi$  and  $S_i$  show the electrostatic potential and the rate of variation of electron density, respectively.

## 2.2 Chemical model

This model incorporates the ground-state species of helium atoms (He), steam molecules (H<sub>2</sub>O), OH molecules, and hydrogen atoms (H). Additionally, excited species above the ground state level have been taken into account. These include helium atoms (Hes), steam molecules (H<sub>2</sub>Os) and OH molecules (OHs), respectively. Moreover, helium ions (He<sup>+</sup>), H<sub>2</sub>O ions (H<sub>2</sub>O<sup>+</sup>), hydrogen positive ions (H<sup>+</sup>), OH positive ions (OH<sup>+</sup>), Oxygen atom (O) and electrons (*e*) have been considered. These species are extremely important due to their presence and applications in He-H<sub>2</sub>O plasma which has been discussed in experimental works [24–27]. The different species included in the plasma model are listed in Table 1. In total, 14 plasma species and 19 distinct processes are all involved in the He-H<sub>2</sub>O mixture. In this model, Tables 2 and 3 provide an extensive overview of the possible reactions that were taken into consideration for helium and H<sub>2</sub>O species.

Generally, surface interactions enable heavy species, such as positive ions, atoms, and metastable atoms to be transferred to the reactor wall. Since negative ions are unable to escape from the ambipolar field or reach to the reactor walls, no surface reactions are required. It is noticed that the only way to extract negative ions from the plasma is interaction with positive ions. This model includes the surface reactions listed in Table 4. Moreover, the decay coefficient rate for neutral particles to the wall surface is calculated using the sticking coefficients.

## 2.3 Boundary conditions and reactions

In this research, the initial magnitude of the electron density in the plasma is constant equal to  $1 \times 10^{13} \text{ m}^{-3}$ , and the densities of neutral species of helium and water molecules are initially considered constant at fractional scales. In addition, the temperature of the gas is considered equal to the room temperature i.e., 300 K. The initial electric potential is in ground state condition i.e., as 0 V, and the initial mean electron energy throughout the whole domain is considered as 5 V. Moreover, the discharge is powered by a Sino negative voltage power source at 750 V.

Here, a dimensional axisymmetric model is utilized to describe the electrical and energetic characteristics of the RF discharge in the He/H<sub>2</sub>O combination. The finite element method is employed for calculating different plasma parameters.

In this research, the simulation's material elements are defined in the air medium by considering the species' pertinent reactions. The Boltzmann's equations are solved and using the cross-sections from the LXCAT data source [28],

rate coefficients were determined. The reaction rates are extracted from different references [24, 25] as mentioned in above tables. One of the electrodes is used in this insulation simulation, and the other one is the same of that.

Here, the electrodes are circular plates with a diameter of 0.1 m. All sections have a predetermined spacing of  $2 \times 10^{-4} \text{ m}$  between the electrode and the insulation, which is the empty area where plasma production occurs. The computational environment for implementing one-dimensional reactor geometry and the related meshes is depicted in Figure 1. Here, the dielectric distance is  $1 \times 10^{-4} \text{ m}$ . For the meshing of the discharge space, a mesh with a symmetrical distribution with element number of 200 and rate of 5 is used. Moreover, for the dielectric space, it is selected from the predefined (extremely fine) mesh with maximum element size of  $3 \times 10^{-6} \text{ m}$ .

## 3. Results and discussion

As referred in different [29, 30], the electron density and its temperature have a significant impact on medical applications. Therefore, in this paper, the main purpose is finding the optimized plasma parameters for utilizing in biomedical surface sterilization. Here, the plasma is a radiofrequency discharge operating at 1 atm pressure. Furthermore, about 20% of the gas combination is made from H<sub>2</sub>O. As a first step, the evolution of the electric potential as a function of distance is shown in Figure 2, in the various percentages of He + H<sub>2</sub>O mixtures like: He + 20% H<sub>2</sub>O, He + 15% H<sub>2</sub>O, He + 10% H<sub>2</sub>O, and He + 5% H<sub>2</sub>O at 0.0015 s. As it is clearly seen in this figure, a concavity is observed in 0. Moreover, the highest magnitudes of electric field are related to He + 5% H<sub>2</sub>O mixture.

In addition, spatial distribution of electron temperature is presented in Figure 3 as a function of different percentages of H<sub>2</sub>O (5, 10, 15, and 20%). As it is obviously seen in Figure 3, the maximum magnitude of temperature is happened at  $sh = 0.1$ . Moreover, at lower positions, a minimum is observed especially at 0.05, but it will be vice versa at higher positions or near to electrode.

A comparison among various voltages and currents of different percentages of H<sub>2</sub>O mixture in He gas is presented in Figure 4. As shown in this figure, an oscillational behavior is appeared for voltage variations. According to the Figure 4, the lowest electric current is obtained at the humidity level of 0.1, which can be caused by more electron collisions at this humidity level, where fewer electrons reach the opposite surface and less current is obtained. These collisions lead to the production of electrons and the density of more positive species. The accumulation of heavy species

**Table 1.** Various species incorporated in the plasma model simulation.

Neutral Species	Exited Species	Ions	Electrons
He	Hes	He <sup>+</sup>	e <sup>-</sup>
H <sub>2</sub> O	H <sub>2</sub> Os	H <sub>2</sub> O <sup>+</sup>	
OH	OHs	OH <sup>+</sup>	
H		H <sup>+</sup>	
O		O <sup>+</sup>	

**Table 2.** List of the main reactions including elastic, excitation, and ionization phenomena [31].

Reaction	Formula	Type	$\Delta\epsilon$ (eV)
1	$e+\text{He}\rightarrow e+\text{He}$	Elastic	0.00
2	$e+\text{He}\rightarrow e+\text{Hes}$	Excitation	19.80
3	$e+\text{He}\rightarrow 2e+\text{He}^+$	Ionization	24.60
4	$e+\text{H}_2\text{O}\rightarrow e+\text{H}_2\text{O}$	Elastic	$3.04 \times 10^{-5}$
5	$e+\text{H}_2\text{O}\rightarrow e+\text{H}_2\text{Os}$	Excitation	$4.59 \times 10^{-1}$
6	$e+\text{H}_2\text{O}\rightarrow 2e+\text{H}_2\text{O}^+$	Ionization	0.13

**Table 3.** List of some reactions with He specie by insertion of rate coefficient [31].

Reaction	Formula	$K^f(\text{m}^3/\text{s.mol})$
1	$\text{Hes}+\text{Hes}\rightarrow e+\text{He}+\text{He}^+$	$1.50 \times 10^{-16}$
2	$\text{Hes}+2\text{He}\rightarrow \text{He}_2\text{s}+\text{He}$	$2 \times 10^{-46}$
3	$\text{H}_2\text{O}+\text{He}^+ \rightarrow \text{He}+\text{OH}+\text{H}^+$	$2.04 \times 10^{-16}$
4	$\text{H}_2\text{O}+\text{He}^+ \rightarrow \text{He}+\text{H}+\text{OH}^+$	$2.86 \times 10^{-16}$
5	$\text{H}_2\text{O}+\text{He}^+ \rightarrow \text{He}+\text{H}_2\text{O}^+$	$6.05 \times 10^{-17}$
6	$\text{H}_2\text{O}+\text{Hes}\rightarrow \text{O}+2\text{H}+\text{He}$	$1.0 \times 10^{-16}$
7	$\text{O}+\text{Hes}\rightarrow \text{He}+\text{O}^++e$	$4.3 \times 10^{-16}$

**Table 4.** Surface reactions with insertion of the sticking coefficient [32].

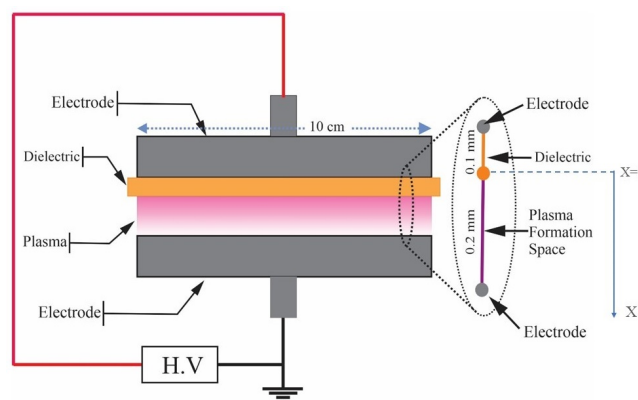
Reaction	Formula	Sticking Coefficient
1	$\text{He}^+ \rightarrow \text{He}$	1
2	$\text{Hes} \rightarrow \text{He}$	1
3	$\text{H}_2\text{O}^+ \rightarrow \text{H}_2\text{O}$	1
4	$\text{H}_2\text{Os} \rightarrow \text{H}_2\text{O}$	1
5	$\text{OH}^+ \rightarrow \text{OH}$	1
6	$\text{H}^+ \rightarrow \text{H}$	1

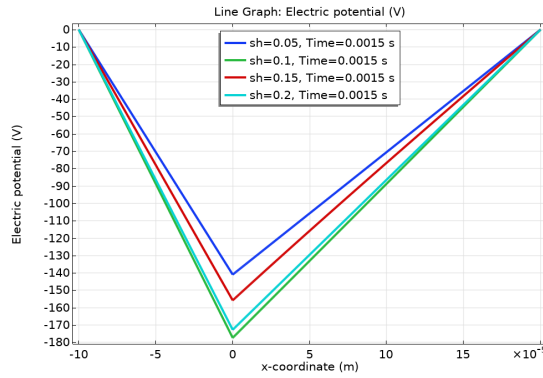
causes the deviation of electrons and causes fewer electrons to reach the opposite plane.

Figure 5 represents the Root Mean Square (RMS) variations of the electron density for different mixtures of  $\text{H}_2\text{O}$  in He gas as a function of distance. A similar trend in magnitudes as seen in Figure 3 can be observed in Figure 5 too. On the other hand, the greatest values in the electron density occur for 0.1 of  $\text{H}_2\text{O}$  similar to the case of the maximum

magnitudes of the electron temperature. In all mixtures, after  $x = 5.0\text{E-}5$ , a growth in electron densities is presented, while a downward trend is shown near to electrode surface. Moreover, a minimum in density is observed for whole  $\text{H}_2\text{O}$  mixture except to 0.1.

The RMS distribution of  $\text{H}^+$  density for various  $\text{H}_2\text{O}$  mixtures in the He gas are shown in Figure 6 as a function of distance. As it is seen in this figure, the greatest magni-

**Figure 1.** A schematic of the structure of the plasma by presenting the locations of the electrodes on the surface and inside of the behind dielectric.



**Figure 2.** The evolution of the electric potential versus distance, for various percentages of H<sub>2</sub>O mixtures of 0.05, 0.10, 0.15, and 0.20.

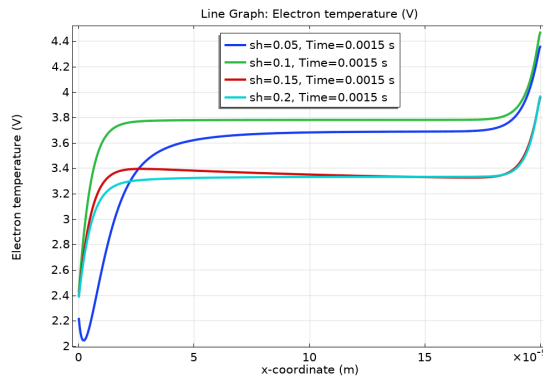


**Figure 3.** The spatial distribution of the electron temperature at 0.0015 s, for different percentages of H<sub>2</sub>O at sh = 0.05, 0.1, 0.15, and 0.2.

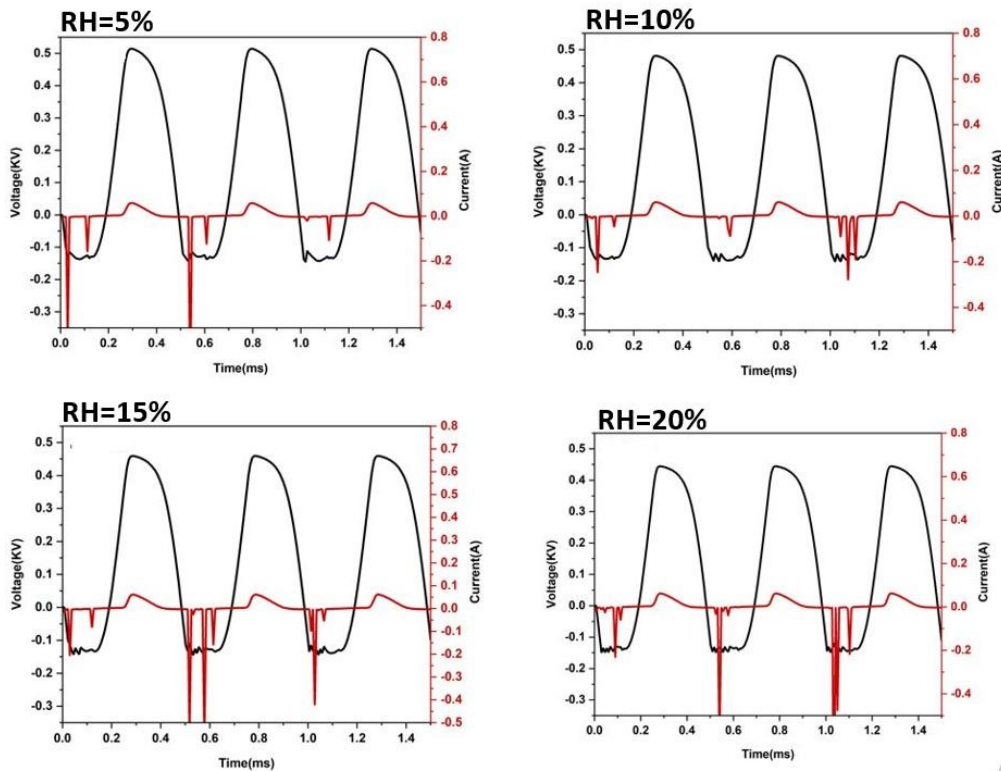


**Figure 4.** The evolution of voltage and current versus time, for different percentages of H<sub>2</sub>O.

tude of  $H^+$  density occurs at 0.1  $H_2O$  and then, a sudden downward trend is observed in this concentration. Furthermore, for two mixtures of 0.1 and 0.15, a decrease in  $H^+$  densities are observed in  $x = 2E-4$ , i.e. in the vicinity of the electrode surface. The numerical value obtained for the electron density for an atmospheric pressure plasma is in good agreement with previous simulation and experimental works [33, 34].

In Figure 7, the evolution of the  $H_2O^+$  density is presented as a function of distance. As it is shown in this figure, the  $H_2O^+$  density for 0.1 mixture has a downward trend. Figure 7 also shows a similar behavior in magnitude to that of Figure 6. As it is seen in this figure, the other percentages represent approximately constant magnitudes with respect to the distance from the electrodes.

The spatial evolution of  $He^+$  density is illustrated in Figure 8 which represents the highest magnitude for 0.1 mixture. Furthermore, at 0.1 mixture, first an increasing trend is seen, but decreasing trend is observed at  $2.0E-4$ . For two percentages of 5% and 20%, a concavity appears at an

approximately distance of  $1.0E-4$  from the dielectric, while for the 15%, the minimum is occurred at  $5.0E-5$ .

The density of excited helium is illustrated in Figure 9. Clearly, at 0.1  $H_2O$  mixture, with highest magnitude show an upward trend between two electrodes. In addition, for all combinations, a drop is presented near the electrode surfaces at  $x = 0$  and  $2E-4$  m. Moreover, at a distance of  $0.75E-4$  from the dielectric, a concavity is presented for two percentages of 5 and 20%.

OH radicals have been reported to enhance chemical processes [35] and can cause damage to the fatty acid side chains of lipids in different membranes, including the mitochondrial membranes of cells [36]. Figure 10 demonstrates the variations of OH density as function of  $x$  coordinate. In this figure for percentage of  $H_2O$  0.1 mixed, a downward trend is represented, especially at distance of  $2E-4$  from the first dielectric. In the other mixtures, a constant density is observed, while at  $2E-4$  meters from the dielectric, all the graphs converged.

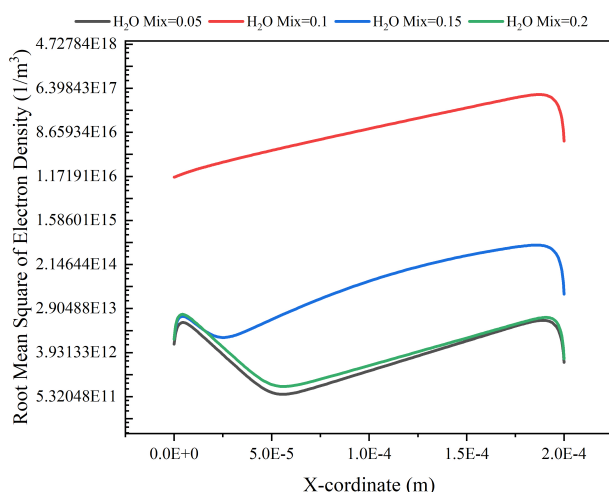


**Figure 5.** The spatial distribution of the electron density for different percentages of  $H_2O$  at  $sh = 0.05, 0.1, 0.15$  and  $0.2$ .

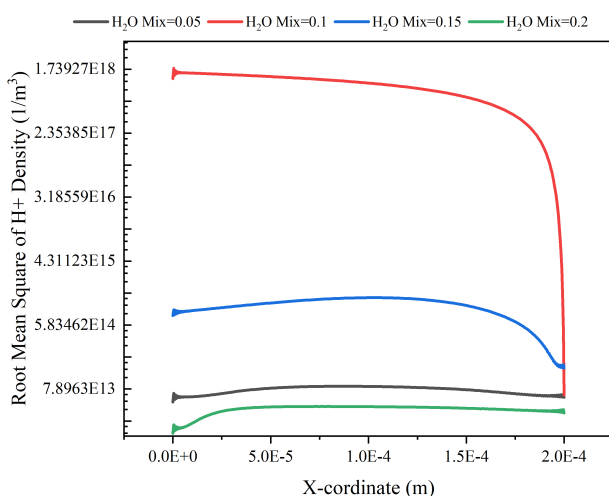


**Figure 6.** The spatial distribution of  $H^+$  density for various  $H_2O$  percentages of  $sh = 0.05, 0.1, 0.15$  and  $0.2$ .

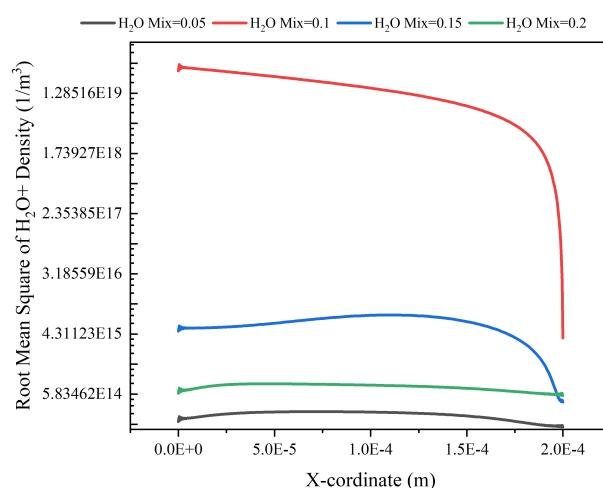


**Figure 7.** The regional distribution of the  $H_2O^+$  density for different  $H_2O$  ratios for various mixtures of  $sh = 0.05, 0.1, 0.15$ , and  $0.2$ .

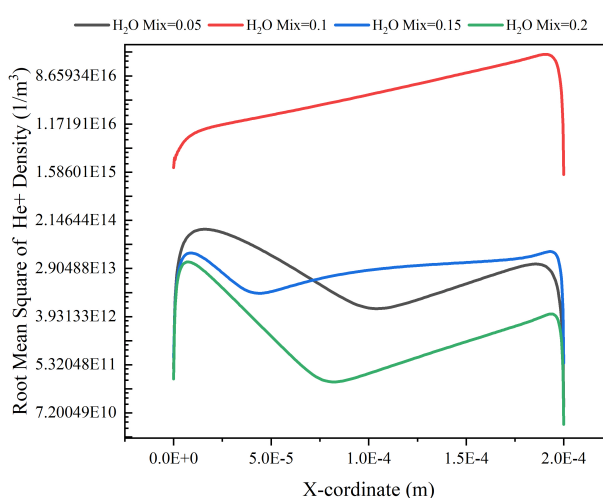


**Figure 8.** The evolution of  $He^+$  density versus distance, for different percentages of  $0.05, 0.10, 0.15$ , and  $0.20$ .

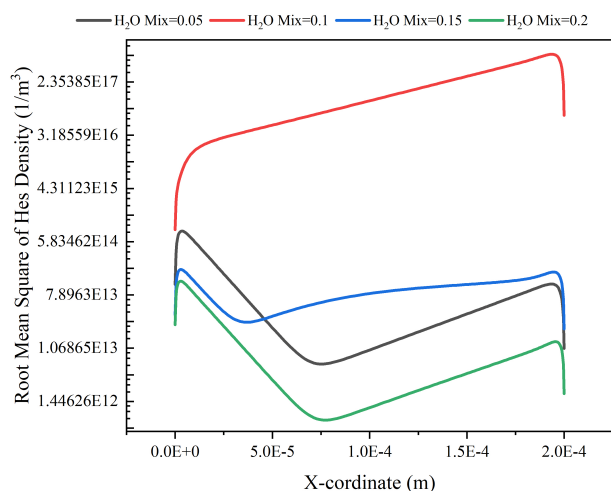


**Figure 9.** The spatial distribution of the exited helium density for different percentages of H<sub>2</sub>O at sh = 0.05, 0.1, 0.15, and 0.2.

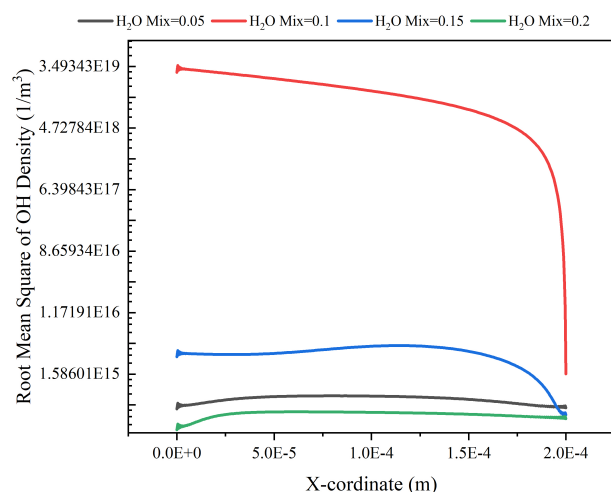


**Figure 10.** Variations of OH density as a function of distance, for different mixtures of H<sub>2</sub>O with 0.05, 0.1, 0.15, and 0.2.

The existence of atomic O, an active species, in plasma-especially cold plasma-is crucial, particularly for applications in medicine. As shown in Figure 11. As the amount of moisture increases, the atomic number of oxygen increases, but this change is not very significant due to the lower contribution.

The amount obtained for the species was compared with previous works. Due to the fact that the plasmas utilized in the earlier studies were specifically tailored for various purposes, the parameters of the plasma, such as voltage, were set at greater levels, thus resulting in an increase in the discharge gap. However, the particle density is directly proportional to the atmospheric pressure plasma of helium-water gas [24, 34, 37].

#### 4. Conclusion

In this paper, research was conducted on the optimized plasma parameters for the generation of radiofrequency discharge plasma under low pressures in a combination of

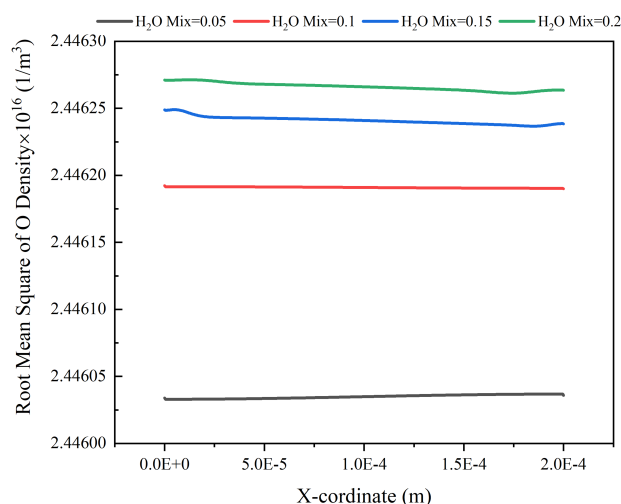


**Figure 11.** Variations of O density as a function of distance, for different mixtures of H<sub>2</sub>O with 0.05, 0.1, 0.15, and 0.2.

helium. The main purpose was to investigate the potential of this plasma discharge in the field of biomedical surface sterilization. Through numerical calculations, the density distributions of various species and the temperatures of electrons during the electrical discharge process were determined. The results showed that the highest magnitudes of electric field were related to He + 5% H<sub>2</sub>O mixture. Furthermore, it was shown that the maximum magnitude of electron temperature was happened at sh = 0.1 or percentage of He + 10% H<sub>2</sub>O mixture. On the other hand, it was found that the highest magnitudes of voltage occurred at 0.05 mixture of H<sub>2</sub>O. In addition, similar to the case of the maximum magnitudes of the electron temperature, it was seen that the greatest values in the electron density occurred for 10% percentage of H<sub>2</sub>O. Moreover, it was found that the highest magnitudes of H<sup>+</sup>, He<sup>+</sup>, Hes (exited helium) and OH<sup>+</sup> densities occurred at 10% H<sub>2</sub>O percentage. Therefore, it was concluded that the best optimization plasma parameters may observe at He with 0.1% H<sub>2</sub>O percentage.

#### Acknowledgement

One of the authors, Ramin Mehradifard, would like to acknowledge the Slovak Research and Development Agency APVV-22-0247 and Comenius University for providing financial support (Grant UK/3032/2024).

#### Authors Contributions

Ramin Mehradifard conceived the presented idea. Zahra Soltani performed the simulation. Ramin Mehradifard and Hamed Soltani completed the simulation. Zahra Soltani wrote the manuscript. Mohammad Mohsen Hatami, Fatemeh Rezaei and Ramin Mehradifard edited the manuscript. Mohammad Mohsen Hatami and Fatemeh Rezaei supervised the findings of this work. All authors discussed the results and contributed to the final manuscript.

**Availability of data and materials**

Data presented in the manuscript are available via request.

**Conflict of Interests**

The author declare that they have no known competing financial interests or personal relationships that could have appeared to influence the work reported in this paper.

**Open Access**

This article is licensed under a Creative Commons Attribution 4.0 International License, which permits use, sharing, adaptation, distribution and reproduction in any medium or format, as long as you give appropriate credit to the original author(s) and the source, provide a link to the Creative Commons license, and indicate if changes were made. The images or other third party material in this article are included in the article's Creative Commons license, unless indicated otherwise in a credit line to the material. If material is not included in the article's Creative Commons license and your intended use is not permitted by statutory regulation or exceeds the permitted use, you will need to obtain permission directly from the OICC Press publisher. To view a copy of this license, visit <https://creativecommons.org/licenses/by/4.0>.

**References**

- [1] Z. Machala and M. J. Pavlovich. "A new phase in applied biology.". *Trends in Biotechnology*, **36**:577–578, 2018. DOI: <https://doi.org/10.1016/j.tibtech.2018.04.001>.
- [2] J. M. Jung, H. K. Yoon, C. J. Jung, S. Y. Jo, S. G. Hwang, H. J. Lee, W. J. Lee, S. E. Chang, and C. H. Won. "Cold plasma treatment promotes full-thickness healing of skin wounds in murine models.". *The International Journal of Lower Extremity Wounds*, **22**:77–84, 2023. DOI: <https://doi.org/10.1177/15347346211002144>.
- [3] S. K. Dubey, S. Parab, A. Alexander, M. Agrawal, V. P. Kumar Achalla, U. N. Pal, M. M. Pandey, and P. Kesharwani. "Cold atmospheric plasma therapy in wound healing.". *Process Biochemistry*, **112**:112–123, 2022. DOI: <https://doi.org/10.1016/j.procbio.2021.11.017>.
- [4] S. Cha and Y. S. Park. "Plasma in dentistry.". *Clinical Plasma Medicine*, **2**:4–10, 2014. DOI: <https://doi.org/10.1016/j.cpm.2014.04.002>.
- [5] R. Mehrabifard, H. Mehdian, and M. Bakhshzadmahmodi. "Effect of non-thermal atmospheric pressure plasma on MDA-MB-231 breast cancer cells.". *Pharmaceutical and Biomedical Research*, **3**:12–16, 2017. DOI: <https://doi.org/10.29252/pbr.3.3.12>.
- [6] R. Mehrabifard, H. Mehdian, K. Hajisharifi, and E. Amini. "Improving cold atmospheric pressure plasma efficacy on breast cancer cells control-ability and mortality using vitamin C and static magnetic field.". *Plasma Chemistry and Plasma Processing*, **40**: 511–526, 2020. DOI: <https://doi.org/10.1007/s11090-019-10050-5>.
- [7] D. Sersenová, Z. Machala, V. Repiská, and H. Gbelcová. "Selective apoptotic effect of plasma activated liquids on human cancer cell lines.". *Molecules*, **26**:1, 2021. DOI: <https://doi.org/10.3390/molecules26144254>.
- [8] D. Dobrynin, G. Fridman, G. Friedman, and A. Fridman. "Physical and biological mechanisms of direct plasma interaction with living tissue. ". *New Journal of Physics*, **11**:115020, 2009. DOI: <https://doi.org/10.1088/1367-2630/11/11/115020>.
- [9] M. Amini, M. Momeni, and A. Jahandideh. "Floating discharge plasma for healing of tendon injury. ". *High Temperature*, **58**:795–799, 2020. DOI: <https://doi.org/10.1134/S0018151X20370014>.
- [10] M. Schröder, A. Ochoa, and C. Breitkopf. "Numerical simulation of an atmospheric pressure RF-driven plasma needle and heat transfer to adjacent human skin using COMSOL.". *Biointerphases*, **10**:029508, 2015. DOI: <https://doi.org/10.1116/1.4916929>.
- [11] X. Lu, Zh. Fang, D. Dai, T. Shao, F. Liu, C. Zhang, D. Liu, L. Nie, and C. Jiang. "On the chronological understanding of the homogeneous dielectric barrier discharge. ". *High Voltage*, **8**:1132–1150, 2023. DOI: <https://doi.org/10.1049/hve2.12382>.
- [12] M. Keidar and I. Beilis. "Plasma engineering: Applications from aerospace to bio and nanotechnology. ". *Academic press*, :442, 2013.
- [13] S. Hajikhani, R. Mehrabifard, and H. Soltani Ahmadi. "A numerical analysis of the impact of gas pressure and dielectric material on the generation of body force in an air gas plasma actuator.". *Radiat. Phys. Eng.*, **5**:51–60, 2024. DOI: <https://doi.org/10.22034/RPE.2024.429773.1176>.
- [14] F. Sohbatzadeh, A. Hosseinzadeh Colagar, S. Mirzanezhad, and S. Mahmodi. "*e. coli*, *p. aeruginosa*, and *b. cereus* bacteria sterilization using afterglow of non-thermal plasma at atmospheric pressure.". *Applied Biochemistry and Biotechnology*, **160**:1978–1984, 2010. DOI: <https://doi.org/10.1007/S12010-009-8817-3/METRICS>.
- [15] J. R. Roth. "Industrial plasma engineering: Volume 2: Applications to nonthermal plasma processing.". *Institute of Physics Publishing*, :1–628, 2001.
- [16] S. Gadkari, X. Tu, and S. Gu. "Fluid model for a partially packed dielectric barrier discharge plasma reactor.". *Physics of Plasmas*, **24**:93510, 2017. DOI: <https://doi.org/10.1063/1.5000523>.

- [17] J. Pan, L. Li, B. Chen, Y. Song, Y. Zhao, and X. Xiu. “Numerical simulation of evolution features of the atmospheric-pressure CF<sub>4</sub> plasma generated by the pulsed dielectric barrier discharge.”. *European Physical Journal D*, **70**:1–8, 2016. DOI: <https://doi.org/10.1140/EPJD/E2016-70081-1>.
- [18] R. Abidat, S. Rebiai, and L. Benterrouche. “Numerical simulation of atmospheric Dielectric Barrier Discharge in helium gas using COMSOL Multiphysics.”. *3rd International Conference on Systems and Control (ICSC)*, :134–139, 2013. DOI: <https://doi.org/10.1109/ICOSC.2013.6750848>.
- [19] Y. B. Golubovskii, V. A. Maiorov, J. Behnke, and J. F. Behnke. “Modelling of the homogeneous barrier discharge in helium at atmospheric pressure.”. *Journal of Physics D: Applied Physics*, **36**:39, 2002. DOI: <https://doi.org/10.1088/0022-3727/36/1/306>.
- [20] S. Tappi, L. Nissen, F. Casciano, G. Antonelli, E. Chiarello, G. Picone, R. Laurita, F. Capelli, M. Gherardi, C. Maccaferri, et al. “Effect of cold plasma generated with different gas mixtures on safety, quality and nutritional aspects of fresh sea bream fillets.”. *Innovative Food Science & Emerging Technologies*, **89**:103477, 2023. DOI: <https://doi.org/10.1016/j.ifset.2023.103477>.
- [21] Y. Ucar, Z. Ceylan, M. Durmusa nd O. Tomar, and T. Cetinkaya. “Application of cold plasma technology in the food industry and its combination with other emerging technologies.”. *Trends in Food Science and Technology*, **114**:355–371, 2021. DOI: <https://doi.org/10.1016/j.tifs.2021.06.004>.
- [22] A. Schmidt, S. Bekeschus, H. Jablonowski, A. Barton, K. D. Weltmann, and K. Wende. “Role of ambient gas composition on cold physical plasma-elicited cell signaling in keratinocytes.”. *Bio-physical Journal*, **112**:2397–2407, 2017. DOI: <https://doi.org/10.1016/j.bpj.2017.04.030>.
- [23] R. Mehrabifard. “Two-dimensional simulation of Argon dielectric barrier discharge (DBD) in plasma actuator structure with COMSOL Multiphysics.”. *Radiation Physics and Engineering*, **4**:43–50, 2023. DOI: <https://doi.org/10.22034/rpe.2023.392080.1127>.
- [24] G. V. Naidis. “Modelling of OH production in cold atmospheric-pressure He-H<sub>2</sub>O plasma jets.”. *Plasma Sources Science and Technology*, **22**, 2013. DOI: <https://doi.org/10.1088/0963-0252/22/3/035015>.
- [25] A. K. Shuaibov, A. I. Dashchenko, and I. V. Shevera. “Emission from a DC glow discharge in a He/H<sub>2</sub>O mixture.”. *Technical Physics*, **46**:1484–1487, 2001. DOI: <https://doi.org/10.1134/1.1418521>.
- [26] X. Pei, Y. Lu, S. Wu, Q. Xiong, and X. Lu. “A study on the temporally and spatially resolved OH radical distribution of a room-temperature atmospheric-pressure plasma jet by laser-induced fluorescence imaging.”. *Plasma Sources Science and Technology*, **22**, 2013. DOI: <https://doi.org/10.1088/0963-0252/22/2/025023>.
- [27] E. Ilik, C. Durmus, and T. Akan. “Adding water droplets into atmospheric pressure plasma jet of helium.”. *IEEE Transactions on Plasma Science*, **47**:5000–5005, 2019. DOI: <https://doi.org/10.1109/TPS.2019.2948701>.
- [28] M. Hayashi. “Electron collision cross-sections for molecules determined from beam and swarm data.”. *Swarm Stud. Inelast. Electron-Molecule Collisions*, :167–187, 1987. DOI: [https://doi.org/10.1007/978-1-4612-4662-6\\_33](https://doi.org/10.1007/978-1-4612-4662-6_33).
- [29] R. Mehrabifard, Z. Kabarkouhi, F. Rezaei, K. Hajisharifi, H. Mehdian, and E. Robert. “Physical understanding of the static magnetic field’s synergistic enhancement of cold atmospheric pressure plasma treatment.”. *arXiv:2304.05833*, :1–23, 2023. DOI: <https://doi.org/10.48550/arXiv.2304.05833>.
- [30] H. Halfmann, N. Bibinov, J. Wunderlich, and P. Awakowicz. “A double inductively coupled plasma for sterilization of medical devices.”. *Journal of Physics D: Applied Physics*, **40**:4145, 2007. DOI: <https://doi.org/10.1088/0022-3727/40/14/008>.
- [31] K. Ding, M. A. Lieberman, and A. J. Lichtenberg. “Hybrid model of neutral diffusion, sheaths, and the  $\alpha$  to  $\gamma$  transition in an atmospheric pressure He/H<sub>2</sub>O bounded rf discharge.”. *Journal of Physics D: Applied Physics*, **47**, 2014. DOI: <https://doi.org/10.1088/0022-3727/47/30/305203>.
- [32] L. C. Pitchford et al. “LXCat: an open-access, web-based platform for data needed for modeling low temperature plasmas.”. *Plasma Process. Polym.*, **14**, 2017. DOI: <https://doi.org/10.1002/ppap.201600098>.
- [33] F. Sohbatzadeh and H. Soltani. “Time-dependent one-dimensional simulation of atmospheric dielectric barrier discharge in N<sub>2</sub>/O<sub>2</sub>/H<sub>2</sub>O using COMSOL Multiphysics.”. *Journal of Theoretical and Applied Physics*, **12**:53–63, 2018. DOI: <https://doi.org/10.1007/s40094-018-0281-4>.
- [34] M. M. Iqbal and M. M. Turner. “Influence of gap spacing between dielectric barriers in atmospheric pressure discharges.”. *Contributions to Plasma Physics*, **55**:444–458, 2015. DOI: <https://doi.org/10.1002/ctpp.201400035>.
- [35] S. Kanazawa, H. Tanaka, A. Kajiwara, T. Ohkubo, Y. Nomoto, M. Kocik, J. Mizeraczyk, and J-S. Chang. “LIF imaging of OH radicals in DC positive streamer coronas.”. *Thin Solid Films*, **515**:4266–4271, 2007. DOI: <https://doi.org/10.1016/j.tsf.2006.02.046>.
- [36] Y. J. Hong, C. J. Nam, K. B. Song, G. S. Cho, H. S. Uhm, D. I. Choi, and E. H. Choi. “Measurement of hydroxyl radical density generated from the atmospheric pressure bioplasma jet.”. *Journal of Instrumentation*,

7:C03046, 2012. DOI: <https://doi.org/10.1088/1748-0221/7/03/C03046>.

- [37] S. Schröter, A. Wijaikhum, A. R. Gibson, A. West, H. L. Davies, N. Minesi, J. Dedrick, E. Wagenaars, et al. “Chemical kinetics in an atmospheric pressure helium plasma containing humidity.”. *Physical Chemistry Chemical Physics*, **20**:24263–24286, 2018. DOI: <https://doi.org/10.1039/c8cp02473a>.